Chapter 5

Multi-colour follow-up with ISAAC

The aim of the initial wide-field survey was to detect EROs with R-J $\geq$5. From our initial survey we selected several fields for multi-colour follow-up with the ISAAC camera at the VLT. In this chapter, we describe the observations and the results of 6 fields for which we have SDSS data available to calibrate the R-band images correctly.

5.1 Observations and data reduction

In order to confirm both the R-J colour and the extended, i.e. non-point-source nature of our pre-selected ERO candidates, we performed multi-band observations with the high-resolution camera ISAAC at the VLT during an observing run in September 1999. We acquired images in both J and K-band (1.2 μm and 2.2 μm respectively) for 6 separate fields. The ISAAC camera has a 150$''$ x 150$''$ field of view and equipped with an 1024^2 pixel Hawaii detector, covering 0.147$''$ pixel^{-1}.
The data were reduced following standard infrared reduction procedures. Each frame was sky-subtracted with temporally adjacent images and then flat-fielded with twilight-sky flats. The combination of header coordinates and, as much as possible, sources in the field was used to determine the offset between the single frames. Each image is a composite of 5 individual exposures, with position offsets in the range of 100 pixels. For source detection, we used only the area covered by all 5 exposures; hence, we lose some of the area due to dithering. In total these data cover approximately 27.1 arcmin^2 .
Table 5.1 summarises the the coordinates and coverage of the 6 fields.

Field name	area [arcmin^2]	RA (h m s)	DEC (^{o} $'$ $''$)
G182_364	4.42	23 53 14.00	+01 09 58.02
G182_474	4.27	23 53 52.00	+01 13 00.94
G202_798	4.39	02 01 06.43	+01 03 49.57
G203_194	4.77	02 10 57.81	-01 07 11.82
G225_0	4.62	21 31 35.90	-00 01 21.71
G248_150	4.58	01 53 12.17	-00 04 57.34

Table 5.1: The 6 ISAAC fields, observed in R, J and K-band.

Adding K-band observations allows us not only to use the R-K $\geq$ 5 colour criterion to detect a larger number of EROs, but also to apply the Pozzetti & Mannucci (2000) classification method, separating old elliptical galaxies from starbursts. In addition, the better seeing conditions (θ_J=0.4..0.5″ for ISAAC, θ_J=1.3..1.6″ for OmegaPrime), provides better morphological information in the two near-infrared bands. The seeing conditions on Cerro Telolo (R-band data) were always worse than during the fullow-up observations with ISAAC, hence, we could not take full advantage of the high quality and the higher spatial redsolution of the ISAAC data (J-band data).

This binning causes some errors in the photometry if one wants to use the "double image" mode of SExtractor. For this reason, we used the positions of all K-band detections as input for the photometry in J and R, allowing for a maximum offset in coordinates of 2 pixels. Allowing such an offset required a careful visual check for wrongly assigned positions and magnitudes.
After combining all three catalogues, we checked each source for the reliability of their coordinates and photometry. Contrary to the ERO catalogue from our R-J survey, this catalogue contains only objects which have been detected in K and R. Each source covers a minimum of 5 pixels, with a detection limit of 3σ above background per pixel (after binning).

5.2 Colour distribution and abundance of the ISAAC sources

The observed fields were originally selected because they were presumed to contain an extremely red galaxy of R-J $\geq$ 5. Due to the corrections necessary to the Metcalfe magnitudes (see section 2.1.1.1), many of these sources did not, in the end, strictly meet our colour criterion. Nevertheles, these objects still have very red optical-to near infrared colours, up to R-K=7.4 (see Figure 5.1 and Table 5.2), and most are certainly redder than the usual R-K$\geq$5 criterion.

Figure 5.1 shows the colour - magnitude distribution of all detections, using the same stellarity criterion for the separation of stars and galaxies as before (stellarity index for galaxies $\leq$0.8.
Applying a colour threshold of R-K$\geq$5 and the stellarity criterion, we selected 15 galaxies (K and R detection) with very red R-K colours up to a magnitude of K$\leq$19.5. The surface density is then:

$$\Sigma = (0.55 \pm 0.14)\ arcmin^{-2} \qquad R - K \geq 5$$

assuming only statistical errors. This result agrees well with Daddi et al. (2002) who found 281 objects in an area of 447.5 arcmin^2, in a comparable magnitude range brighter than K=19.2. In comparison, we calculated the surface density of EROs with R-J$\geq$5 and J<20.5 as (section 4.3.1):

$$\Sigma = (0.97 \pm 0.07) \times 10^{-2}\ arcmin^{-2} \quad R - J \geq 5$$

In order to use the classification method from Pozzetti & Mannuccci, discussed in section 3.4, we used the coordinate list from all K-band detections to search for objects in J. The positions of these sources were than the starting point for R-band photometry, also in a search radius of 2 pixels.

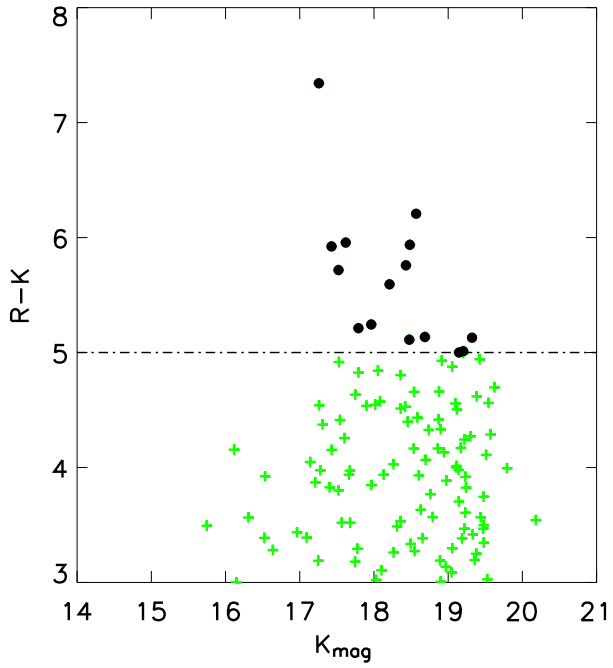

Figure 5.1: R-K colour versus K magnitude for ISAAC detections. All objects have been classified as galaxies, i.e. stellarity ≤ 0.8.

In the following section we will combine the K and R-band data with the J-band observations, also obtained with ISAAC. Having both the R-K and J-K colour, we apply the colour-colour classification by Pozzetti & Mannucci (2000), to distinguish between ellipticals with an old stellar population and dusty starbursts.

5.3 The Abundance of old ellipticals and dusty starbursts

The motivation for the increasing number and depth of near-infrared surveys for studying the high redshift galaxy population was to constrain models of galaxy formation and evolution, by comparing these models with observed abundances of galaxy types. Applying a colour threshold of R-K$\geq$5, which is commonly used to select the ERO population at intermediate redshift (1$<$ z $<$2), we select old ellipticals, dusty starbursts, or disk dominated galaxies, reddened by large amounts of dust in the line of sight.
Numerous other surveys have found an almost equal distribution between old ellipticals and starburst galaxies (e.g. Cimatti et al. 2002a, Mannucci et al. 2002). The colour-colour diagrams in Figure 5.2 show the distribution of all 13 sources, detected in K, J and R-band, with R-K$\geq$5, both in the R-K and R-J *vs.* J-K colour plane. The dashed line represents the separation between old ellipticals and dusty starbursts, as described by Pozzetti & Mannucci (2000).
Although the number of EROs is relatively small, their colour distribution (see Figure 5.2) agrees well with the assumption of a dominance of evolved ellipticals among this ERO population (Moriondo et al. 2000, Cimatti et al. 1999).

Both panels in Figure 5.2 show an exceptional red object, R-K= 7.44 and R-J=6.47, at a very blue J-K colour. In the R-K *vs.* J-K colour plane, this object lies in a range of R-K which is normally assigned to stellar objects (Pozzetti and Mannucci 2000 & Mannucci et al. 2002). However, while the images of this object (panel i) in Figure 5.3 in J and K reveal a very compact object, the R-band detection shows an elongated structure. The limited resolution in R does not allow for a more detailed description of the morphology. As we can see from Figure 5.3, the near-infrared images also permit no discrimination between the different morphological galaxy types; this would require higher spatial resolution.

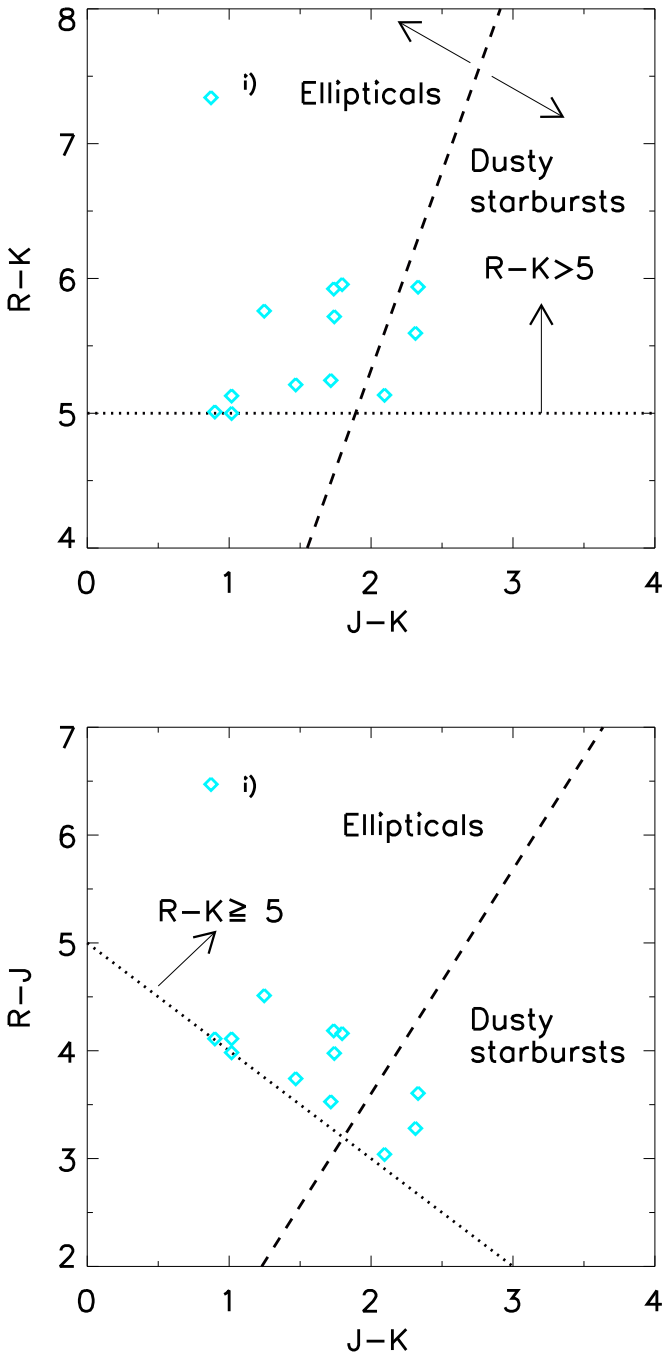

Figure 5.2: R-K and R-J colour *vs.* J-K colours for the 13 sources which exceed the R-K ≥ 5 colour criteria for massive galaxies at z>1 (Roche et al. 2002 & Daddi et al. 2000). The dotted lines show the R-K$\geq$ 5 colour limit, while the dashed line is the separation of old ellipticals and dusty starbursts of Pozzetti & Mannucci (2000). Note the very red object labelled (i) which is discussed further in the text.

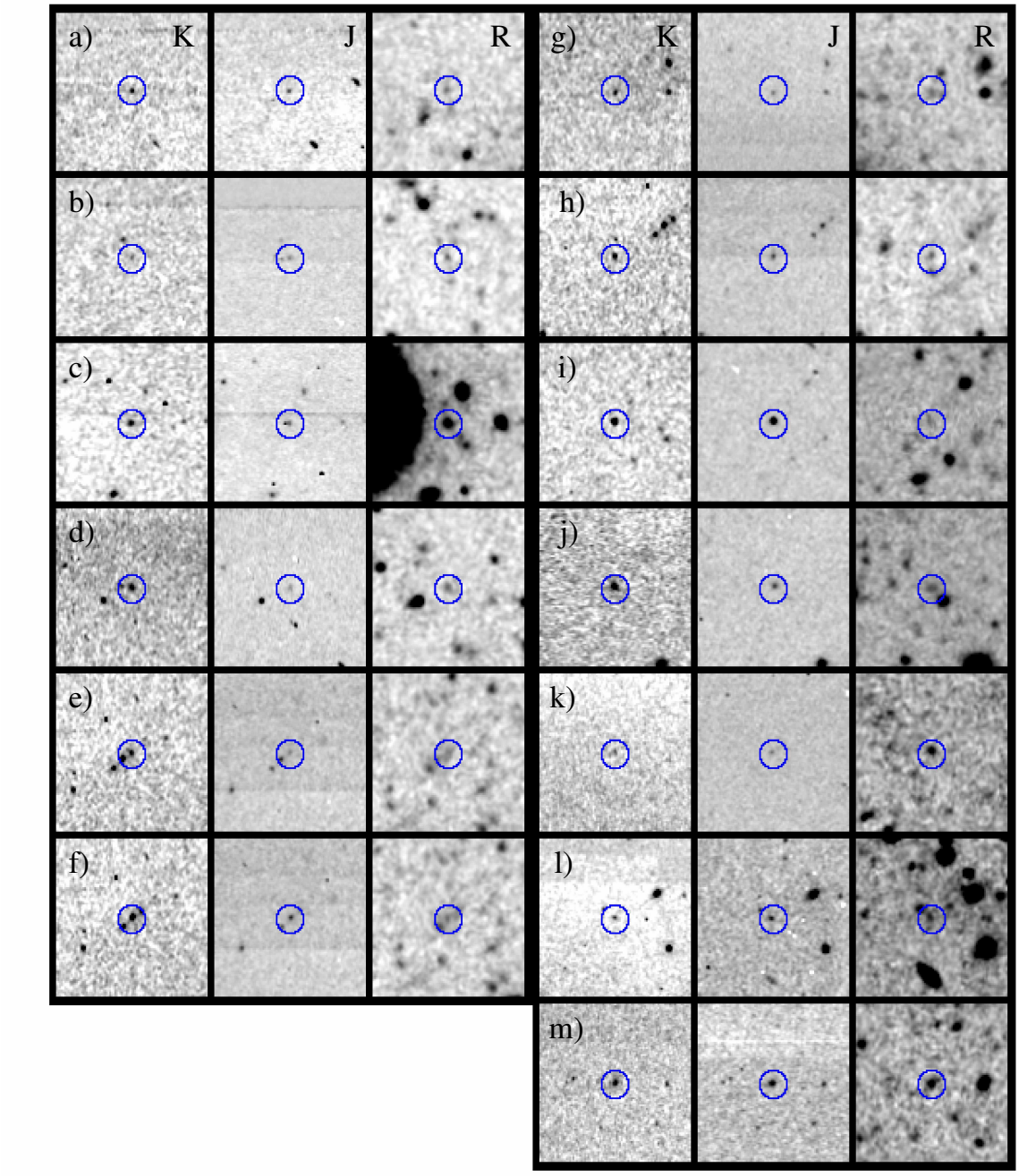

Figure 5.3: Images of all 13 ISAAC EROs (R-K≥5) in K, J and R-band. Each image is 35″ square.

Image ID	Field	K [mag]	K_{stell}	J [mag]	J_{stell}	R[mag]	R_{lim}	R_{stell}	R-K	R-J	J-K
a)	G182_364	18.48	0.00	20.81	0.02	24.42	25.20	0.35	5.93	3.60	2.33
b)	G182_474	19.32	0.00	20.33	0.00	24.45	25.20	0.31	5.12	4.11	1.01
c)	G182_474	17.79	0.00	19.26	0.02	23.00	25.20	0.00	5.21	3.74	1.46
d)	G202_798	18.21	0.00	20.52	0.00	23.80	24.70	0.00	5.59	3.28	2.31
e)	G202_798	17.96	0.00	19.68	0.00	23.20	24.70	0.00	5.24	3.52	1.71
f)	G202_798	17.43	0.02	19.16	0.00	23.35	24.70	0.00	5.92	4.18	1.73
g)	G202_798	18.68	0.00	20.78	0.00	23.82	24.70	0.01	5.13	3.04	2.09
h)	G202_798	18.43	0.01	19.67	0.00	24.19	24.70	0.57	5.75	4.51	1.24
i)	G203_194	17.25	0.05	18.12	0.03	24.61	24.60	0.33	7.34	6.47	0.87
j)	G203_194	17.52	0.01	19.26	0.02	23.23	24.60	0.00	5.71	3.97	1.74
k)	G248_150	19.20	0.05	20.10	0.00	24.21	25.10	0.01	5.01	4.11	0.89
l)	G248_150	19.14	0.00	20.16	0.00	24.14	25.10	0.10	5.00	3.98	1.01
m)	G248_150	17.62	0.01	19.41	0.02	23.57	25.10	0.02	5.95	4.16	1.79

Table 5.2: Photometric informations on all sources with R-K$\geq$5. The first column refers to the numeration in Figure 5.3.

Nevertheless, the images in Figure 5.3 clearly demonstrate the necessity for follow-up observations with instruments like ISAAC. While OmegaPrime detected only a single source (left panel in Figure 5.4), observations with ISAAC resolved 3 objects, two of these sources have relative red colours (R-K= 5.24 and 5.92, labelled (e) and (f) in Figure 5.3). In addition we found another red object (R-K$\geq$5.75) less than 17″ away, which was not detected with OmegaPrime.
Considering the apparent alignment of these objects, it will be interesting to obtain redshift estimates for each component, indicating whether or not these belong to a bound system.

This example clearly shows the need for deeper follow-up observations on the pre-selected ERO candidates, especially in respect to the confirmation of a galaxy cluster. Due to the necessary binning of the ISAAC near-infrared data, we can not use the higher spatial resolution of ISAAC. However, the better seeing conditions at the VLT (ISAAC: seeing=0.55 arcsec, OmegaPrime: seeing=1.23 arcsec in J), facilitate the detection of multiple EROs while OmegaPrime detected only one single ERO (Figure 5.4). Therefore, additional follow-up observations will require equally good conditions like the previous ISAAC observations.

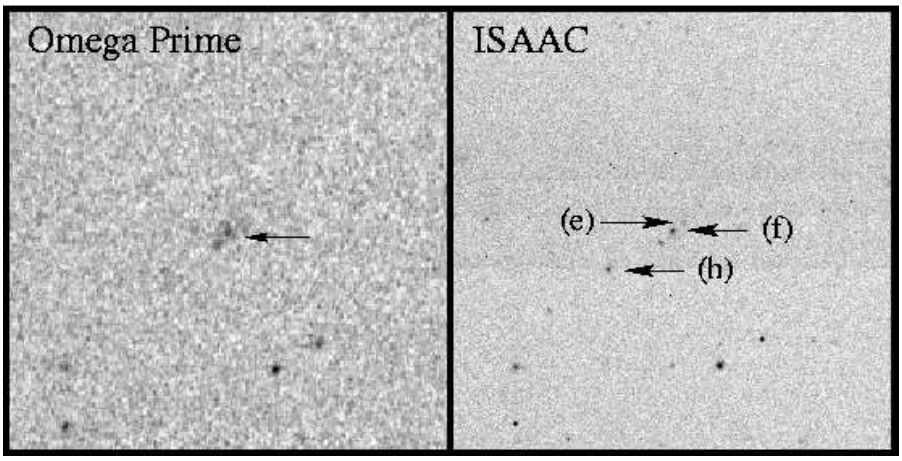

Figure 5.4: This ERO has been detected in J during the observations with the OmegaPrime camera at the 3.5m telescope at Calar Alto (left panel). Both images are 80 ″ in size, but have different pixel scales: OmegaPrime: 0.396″/pixel; ISAAC: 0.147 ″/pixel. We clearly detect three objects, two of them classify as ERO with R-K = 5.24 (e) and 5.92 (f) .